Journal: **PHILOSOPHICAL TRANSACTIONS OF THE ROYAL SOCIETY A**

Article id: **RSTA20140350**

Article Title: **Efficient preliminary floating offshore wind turbine design and testing methodologies and application to a concrete spar design**

First Author: Denis Matha

Corr. Author(s): Denis Matha

AUTHOR QUERIES – TO BE ANSWERED BY THE CORRESPONDING AUTHOR

As the publishing schedule is strict, please note that this might be the only stage at which you are able to thoroughly review your paper.
Please pay special attention to author names, affiliations and contact details, and figures, tables and their captions.
If you or your co-authors have an ORCID ID please supply this with your corrections. More information about ORCID can be found at http://orcid.org/.
No changes can be made after publication.

The following queries have arisen during the typesetting of your manuscript. Please answer these queries by marking the required corrections at the appropriate point in the text.

Q1	Please confirm whether 'look-up table' refer to table 1.
Q2	Please edit the sentence 'The general form of the solution for. . .' for clarity.
Q3	Please provide report number for ref. [10].
Q4	Please provide location details for Refs [12,13,32,44].
Q5	Please provide publisher location for ref. [32].

PHILOSOPHICAL TRANSACTIONS A

rsta.royalsocietypublishing.org

Research

Cite this article: Matha D, Sandner F, Molins C, Campos A, Wen Cheng P. 2015 Efficient preliminary floating offshore wind turbine design and testing methodologies and application to a concrete spar design. *Phil. Trans. R. Soc. A* 20140350.
http://dx.doi.org/10.1098/rsta.2014.0350

One contribution of 17 to a theme issue 'New perspectives in offshore wind energy'.

Subject Areas:
mechanical engineering, ocean engineering, structural engineering, energy

Keywords:
floating offshore wind turbines, design, monolithic concrete spar buoy, combined wind wave testing, AFOSP

Author for correspondence:
Denis Matha
e-mail: matha@ifb.uni-stuttgart.de

THE ROYAL SOCIETY PUBLISHING

Efficient preliminary floating offshore wind turbine design and testing methodologies and application to a concrete spar design

Denis Matha[1], Frank Sandner[1], Climent Molins[2], Alexis Campos[2] and Po Wen Cheng[1]

[1]Stuttgart Wind Energy, University of Stuttgart, Stuttgart, Germany
[2]Department of Construction Engineering, Universitat Politècnica de Barcelona, Barcelona, Spain

The current key challenge in the floating offshore wind turbine industry and research is on designing economic floating systems which can compete with fixed-bottom offshore turbines in terms of levelized cost of energy. The preliminary platform design, as well as early experimental design, assessments are critical elements in the overall design process. In this contribution, a brief review of current floating offshore wind turbine platform pre-design and scaled testing methodologies is provided, with a focus on their ability to accommodate the coupled dynamic behaviour of floating offshore wind systems. The exemplary design and testing methodology for a monolithic concrete spar platform as performed within the European KIC AFOSP project is presented. Results from the experimental tests compared to numerical simulations are presented and analysed and show very good agreement for relevant basic dynamic platform properties. Extreme and fatigue loads and cost analysis of the AFOSP system confirm the viability of the presented design process. In summary, the exemplary application of the reduced design and testing methodology for AFOSP confirms that it represents a viable procedure during pre-design of floating offshore wind turbine platforms.

1. Introduction

Floating offshore wind turbines (FOWTs) represent a promising technology to enable economic offshore

wind electricity generation in deep waters beyond 50 m. Hywind [1,2], WindFloat [3–6] and Fukushima-FORWARD Phase 1 [7] prototypes have demonstrated the technical feasibility of multi-megawatt floating wind turbines. Projects focused on numerical tool development and code comparison such as the international OC3, OC4 and OC5 projects (IEA Wind Tasks 23 and 30) and European research projects such as UpWind have shown the tools' capability to sufficiently numerically represent the physics of FOWT systems. The current key challenge in FOWT industry and research is on designing economic floating systems which can compete with fixed-bottom offshore turbines in terms of levelized cost of energy [8–11]. To achieve that ambitious target, apart from novel challenges regarding installation, operation, maintenance and logistics, the preliminary platform and turbine controller design, as well as early experimental design, assessments are key elements in the overall design process. That challenge is not only economic but the design problem serves as an overarching theme for focused research and is strongly related to questions regarding the required numerical model fidelity, i.e. identifying the right balance between computational efficiency, accuracy and suitability for innovative integrated optimization methodologies, as well as the quantification of physical models' limitations and their further development. In this paper, an overview of current FOWT platform pre-design and scaled testing methodologies is provided, with a focus on their ability to accommodate the coupled dynamic behaviour of floating offshore wind systems. To illustrate the process an exemplary design and testing methodology for a monolithic concrete spar platform as performed within the European KIC AFOSP project is presented. Additionally, experiences gained from the ongoing EU Fp-7 INNWIND.EU are incorporated. In the first section, the pre-design FOWT process is outlined and in the second section, the process is illustrated with a description of the pre-design performed in AFOSP and the important physical principles, models and associated equations used. The third section provides an overview about current FOWT testing methodologies and explains the issues related to simultaneous wind and wave testing and the difficulties of preservation of dimensionless numbers. It is followed by an illustration of the reduced but efficient testing procedure as applied in AFOSP.

2. Pre-design process

Pre-design as a term is here used to describe the definition of all main platform properties (such as geometry, mass distribution) including a global loads analysis according to design load cases (DLC) [12] but excluding any details related to industrialization and manufacturing such as detailed local structural stress analyses, O&M and marine operations procedures.

Typically, the floating substructure consisting of the platform and mooring system is designed to comply with existing FOWT-specific guidelines and standards such as those in [13,14] and the therein referenced standards for floating offshore Oil and Gas structures. In addition to requirements typical for any offshore floating structure such as system natural frequencies and related response amplitude operators (RAOs) placed off the wave peak spectral frequencies at the considered site (heave, roll and pitch eigenperiods below 3–5 s or above 25–30 s), a draft and mooring system suitable for the considered location and soil condition, and generally a minimal sensitivity to wave excitation forces, FOWT-specific requirements originating from the aerodynamic forces acting on the selected tower and rotor-nacelle assembly (RNA), structural and aeroelastic coupling effects and interactions with the control system need to be taken into account. This includes that the system withstands the mean and dynamic thrust force on the rotor without exceeding the limiting static and dynamic platform heel angles and accelerations and does not exceed ultimate and fatigue limit states (FLSs) in any design load condition at the specific site. The overall target of the design is to arrive at a competitive levelized cost of energy (LCOE, €/kWh), which is the dominating and decisive factor in the renewable offshore wind energy sector. To achieve that target numerical and experimental methods with different levels of complexity and sophistication is necessary. In the pre-design stage, the focus is on efficient methods based on simplified, conservative, proven physical models.

In practice, first the platform type (ballast, buoyancy, mooring stabilized) and general hull geometry based on a list of (site-dependent) requirements is selected. Then simple hydrostatic analyses are performed yielding the continuous, not discretized design space and appropriate hydrostatic properties so that relevant structural quantities like mass, centre of mass, moment of inertia and mooring line restoring stiffness can be formulated. Already at this stage, material and manufacturing costs are estimated for all possible designs fulfilling the requirements to approximate the capital expenditure (CAPEX) and optimize the design. Based on the basic geometry from the hydrostatic computations, potential flow hydrodynamic frequency domain panel solvers are applied with regular waves using a preliminary conceptual mooring system to obtain wave RAO and hydrodynamic coefficients, represented in terms of added mass A ($n_{\mathrm{frq}} \times 6$) and radiation damping B ($n_{\mathrm{frq}} \times 6$) for the sinusoidally oscillating platform (manoeuvring/radiation problem). The panel code is also used to compute the incident-wave frequency-dependent wave excitation vector $X(n_{\mathrm{frq}} \times n_{\mathrm{wavedir}} \times 6)$ (seakeeping/diffraction problem). With A, B, C and X, dynamic time-domain simulations of the platform can be set up and performed applying linear hydrodynamic theory assuming a rigid floating body. The mooring system design is defined by selecting the line properties, number of lines and their topology to enable the set-up of quasi-static or dynamic mooring line models. The radiation, diffraction and added mass dynamic properties are influenced by the platform hull shape only. If the designer does not want to alter the general geometry, additional hydrodynamic features can be used to improve the design. For the adjustment of the added mass properties, heave plates are a common option [5]. The potential flow panel solvers inherently do not account for viscous effects, so the viscous damping is difficult to estimate without experimental data or advanced simulations. However, dependent on the significant dimensions of the platform and the wave kinematics an *a priori* classification of the relative importance of viscous or diffraction effects is possible and can be taken into account by using literature values or simplified approximations [15]. Except for tension leg platforms (TLPs), the mooring system dynamics have limited influence on the platform at this design stage and may be sufficiently represented in a simplified way with a linear spring stiffness acting on the overall centre of mass of the system [16]. The adjustment of the mooring restoring characteristics can be a convenient parameter for system optimization in further design stages. In the later design stages, the mooring system needs to be designed according to recognized standards such as ISO19901-7.

At this point in the design, assuming that the RNA and initial tower properties are given, aero-hydro-servo-elastic numerical models of varying fidelity can be set up to perform coupled linear and dynamic analysis in realistic conditions and identify critical DLC. Owing to the possible introduction of negative damping for the FOWT from the onshore RNA blade pitch control system [17], the pitch controller of the RNA needs to be adapted. Starting either from an existing onshore controller or a new baseline PI-controller design, innovative integrated controller optimization methods can be applied based on sequential optimization of controller properties by linear and nonlinear system analysis of the coupled system [16]. Also typically the initial tower design based on the onshore or fixed-bottom design is modified once the platform is completely defined and results from the dynamic load analysis are available. It shall be noted that the assumption of known data for the wind turbine in practice is often not fulfilled owing to confidentiality constraints between the platform designer and RNA manufacturer—in such a case simplified assumptions regarding the RNA, such as thrust and moment coefficient curves are a solution. Also in the future inclusion of not only the controller but also the RNA design into the FOWT design process may lead to further improvements.

In parallel to the DLC simulations, multiple experimental wind and/or wave tank test campaigns are usually performed to confirm numeric simulations results, adjust the used hydrodynamic coefficients, check critical cases and additional complex components such as heave plates and secondary structures and quantify model uncertainties. A more detailed LCOE cost tool, including CAPEX and operational expenditure (OPEX), can be set up to serve as a supporting tool in the design optimization process, particularly to formulate viable cost functions. At this stage, the pre-design is completed and the whole process may be repeated a number of times

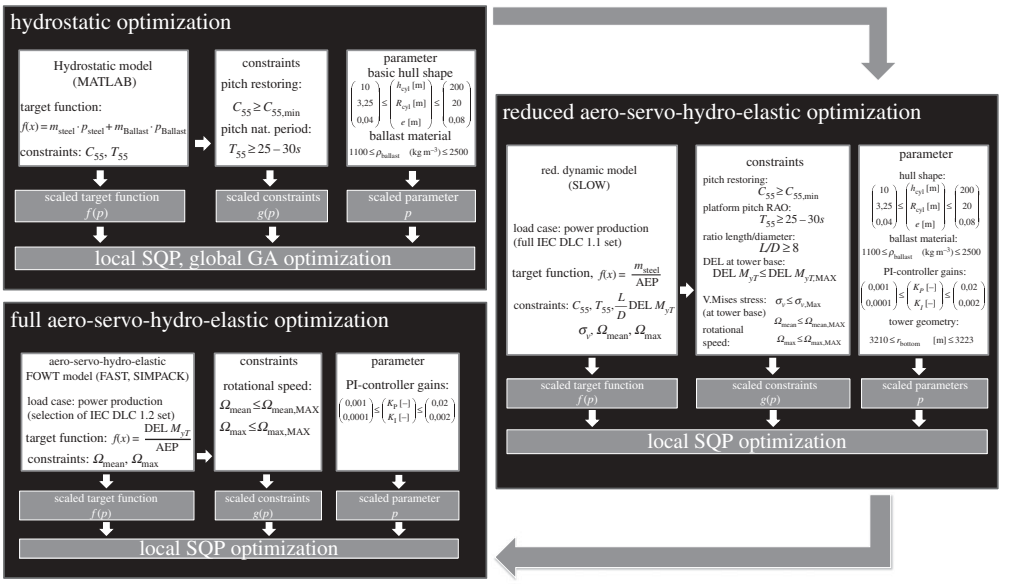

Figure 1. Three-staged FOWT optimization method (adapted from [18]).

to arrive at the final pre-design, where no more major changes to design are applied in the subsequent steps.

For the design iteration several methods are applicable. The most general method is by using appropriate global optimization schemes with elaborate cost functions encompassing all outlined pre-design steps; yet this may be computationally inefficient and also disregards the designers knowledge. A variation thereof is to sequentially and separately optimize the design in each design stage [18] applying gradient based or evolutionary optimization algorithms, as depicted in more detail in figure 1 for an exemplary optimization of the OC3-Hywind spar using a local nonlinear sequential quadratic programming and a global genetic algorithm (GA)-based optimization method.

In the process presented in figure 1, the first hydrostatic optimization stage for the basic platform geometric and mass properties is focused on reducing structural and ballast mass while fulfilling the constraints in hydrostatic pitch restoring and platform pitch eigenperiod. During the second optimization stage, the previously described reduced nonlinear dynamic model is applied with the target to reduce mass and at the same time increase annual energy production (AEP). Here constraints on rotor speed, damage equivalent load (DEL) and equivalent tensile stress at the tower base and the ratio of platform length and diameter are defined in addition to the previous ones. In this stage, in addition to hull shape and mass distribution, the controller gains and tower structure is optimized. Note that in the shown second-stage optimization, as well as for AFOSP, the hydrodynamics are computed by Morison's equation (3.5) allowing for easy changes of the hull shape. For hydrodynamic models requiring panel code pre-calculations of A, B, C and X, this process is more demanding and requires a parametrization of the panel code (this methodology is currently applied for the platform design within the INNWIND.EU project). The third optimization stage applies the detailed aero-hydro-servo-elastic numerical model for a few selected DLCs to further optimize the controller gains to minimize the fatigue load at the tower base and increase AEP. This exemplary procedure is very flexible and adaptable to specific design criteria by modifying the target functions, constraints and parameters that are optimized. However, the approach giving the designer most control about the process is to manually select discrete candidate designs in each stage according to defined target criteria and narrowing down the selection in each consecutive analysis to arrive at a final pre-design concept.

With the final pre-design and experimentally validated numerical models, critical load cases may be reviewed with advanced software tools or dedicated experiments in order to e.g. check the behaviour in nonlinear waves and green water, quantify second and higher order hydrodynamic effects or investigate the potential for ringing or vortex-induced vibrations (VIV). Next the detailed component design including structural dimensioning based on global loads from coupled simulations and decoupled local stress analyses according to offshore standards is performed, e.g. using scantling equations. Also the detailed manufacturing and installation process, maintenance, logistics, health and safety, environmental and legislation aspects are addressed. Detailed design studies specific to FOWT can be found in the literature, e.g. for a semi-submersible FOWT [19–21], a spar FOWT [22,23] and a TLP FOWT [24,25]. A general design process for offshore structures is outlined in [26].

3. AFOSP monolithic concrete spar design

To illustrate the design process outlined in the §2, the pre-design conducted in the European KIC-InnoEnergy project AFOSP (Alternative Floating Platform Designs for Offshore Wind Turbines using Low Cost Materials) is presented in this section (a similar design process is also used within the European INNWIND.EU project, finishing in 2017). In AFOSP a new concept of a floating spar platform was developed [22,27–29] by a consortium of Gas Natural Fenosa, University of Stuttgart and Universitat Politècnica de Catalunya from 2012 to 2014. In contrast to existing spar FOWT prototypes, the AFOSP design is a monolithic structure including both the platform and the tower and uses post-tensioned concrete as main material. This leads to less material cost and an extended lifetime up to 60 years, resulting in a lower CAPEX than equivalent steel spar designs. The internal forces distribution in the spar structure is convenient from the point of view of durability including fatigue and chemical or physical attack. Other solutions such as semi-submersibles or TLPs, if built in concrete, require more complex structural parts which are subjected to large tension forces, making it very difficult to assure full compression stresses in all structural members. If some members are subjected to tension stresses, the fatigue resistance is highly affected as well as the appearance of cracks dramatically accelerates the water and chlorides penetration, reducing the durability of the structure.

Figure 2 schematically presents the design process that was applied for the AFOSP design, which supports the NREL 5 MW wind turbine [30]. Following the concept selection, the initial platform properties for the spar's draft, base and waterplane diameter, position of centre of mass and buoyancy and mooring line stiffness were primarily defined to yield a specific hydrostatic restoring stiffness C_{55} in platform pitch direction, part of the overall hydrostatic stiffness matrix $C_{\text{hydrostatic}}$. This target value $C_{55} = 1.4 \times 10^9\,\text{Nm rad}^{-1}$ is determined by the maximum acceptable static platform heel angle at maximum rotor thrust of the NREL 5 MW WT [30], specified at 5° for AFOSP. C_{55} is an important site-independent platform parameter because it directly influences the mean platform heel angle which affects the AEP by a cosine relationship: $\text{AEP} \sim \cos(\beta)^3$. The chosen 5° maximum design heel angle for AFOSP corresponds to less than 1% of AEP reduction, which was considered acceptable. Equation (3.1) describes a simple way to estimate the linearized hydrostatic restoring stiffness C_{55} of the whole FOWT multi-body system about y about the seawater level (SWL) with various bodies i with their centre of mass located at z_i above SWL

$$C_{55} = \sum -z_i m_i g + M_{\text{wtrpln}} + z_{\text{COB}} m_{\text{FOWT}} g + C_{\text{Lines}}. \tag{3.1}$$

M_{wtrpln} denotes the waterplane area restoring calculated using the second moment of area of the horizontal cross-section at SWL [31]. The restoring from the mooring system C_{Lines} is of limited importance for spar designs at this stage and can be well represented as a linear stiffness. By application of a gradient-based optimizer and variation of the platform parameters, the multi-dimensional design space for a constant C_{55} can be computed to define a selection of candidate designs as presented in figure 3 with varying radii (r_{spar}), drafts (l_{spar}), platform periods (T_{55}) or mass distributions (m_{FWT}, $M_{55/55a}$); note that figure 3 does not show the AFOSP design space but

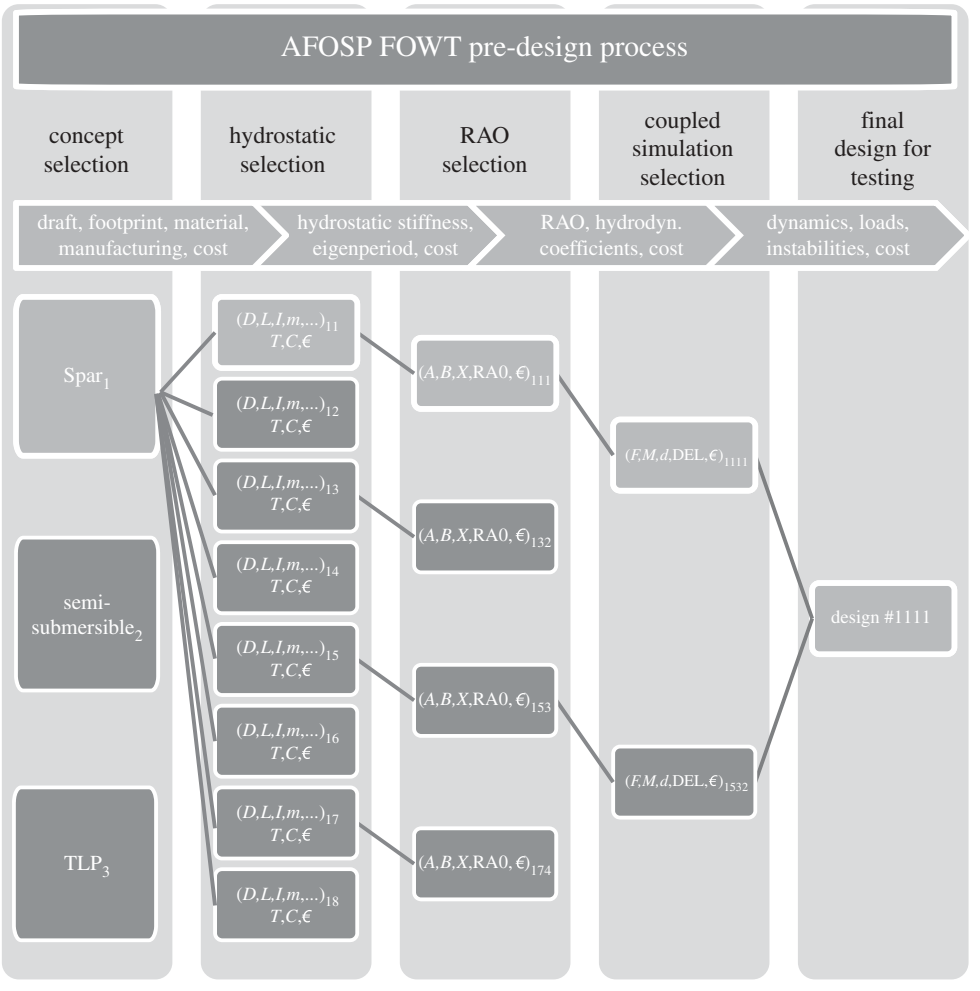

Figure 2. AFOSP design process.

of a generic steel spar design. In further design steps, the nonlinear hydrostatic restoring can be computed in order to assess the restoring properties for larger pitch angles [32].

To ensure that the still water eigenperiod, which (to some extent) is correlated to the RAO peak frequency, is out of the wave excitation resonance a minimum value of $T_{\mathrm{eig,min}} = 25\,\mathrm{s}$ should not be undercut [26]. In AFOSP, an initial estimate for the system's pitch eigenperiod $T_{\mathrm{eig,55}}$ was computed by applying equation (3.2) with the mass moment of inertia in pitch M_{55} of the system and an estimated additional mass moment of inertia of the platform in pitch from the added mass A_{55} [5]. The quantities in the equation (3.2) are formulated around the estimated centre of rotation of the FOWT, typically assumed as the overall system centre of mass or the centre of buoyancy [33].

$$T_{\mathrm{eig,55}} \approx \frac{2\pi}{\sqrt{C_{55}/(M_{55} + A_{55})}}. \tag{3.2}$$

Owing to the significantly greater displaced water mass and therefore much larger added inertia of a concrete spar compared with a dynamically equivalent steel design, the eigenperiods for all AFOSP candidate designs in stage 2 were out of the critical range and therefore were identified as quantities that could be neglected at this stage of the AFOSP design process.

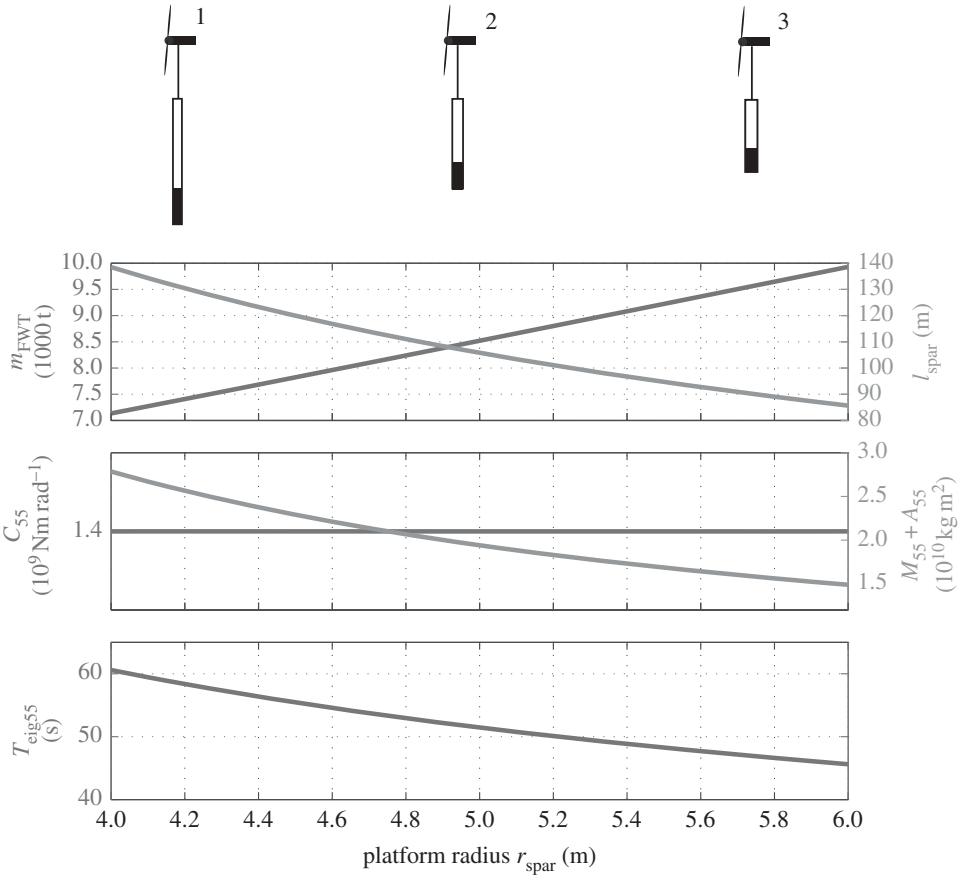

Figure 3. Multi-dimensional design space [16].

Based on the range of system properties that satisfy the constraint prescribed for the pitch restoring and system eigenperiod the design space was defined. Then specific AFOSP candidate designs were selected based on the estimated CAPEX (based on platform mass). For spar designs as can be identified in the top diagram of figure 3, a small radius is generally decreasing mass and CAPEX. At the same time, a decreasing radius leads to a more slender spar with larger draft. This reduces the potential addressable market because it limits the concept in terms of minimum required water depth and also is less favourable in terms of structural stresses. Particularly at the transition from tower to platform, the internal bending stresses are maximum and additional expensive steel reinforcements may be required for a more slender platform, ultimately offsetting the initial mass reduction. Wall thicknesses of members can only be optimized to some extent owing to structural and constructive requirements and require multiple detailed internal stress analyses and simulations. An accurate estimate in terms of cost for these trade-offs is difficult in this early design stage, so for AFOSP a number of candidate designs were initially chosen covering a range of different reasonable combinations of platform draft and radius based on simplified cost assumptions and engineering judgement.

An incorporation of this candidate selection into an automated optimization approach as outlined in figure 1 for the OC3-Hywind Spar buoy was not performed in case of the AFOSP design, but would in general be feasible. This decision was made due to the difficulty and error-proneness of developing an appropriate cost function economically quantifying the relations between draft and addressable market, radius and dynamic behaviour and internal stresses. Additionally, automated optimizations always carry a large computational overhead by computing unreasonable combinations that can be excluded in a manual design process.

Following the hydrostatic selection, in the third design stage all selected AFOSP candidate designs are analysed in the hydrodynamic panel code ANSYS AQWA to compute the RAOs, as well as the frequency-dependent linear hydrodynamic coefficients, added mass A, radiation damping B and the wave excitation vector X. It allows selecting a platform with an RAO with low magnitude off the peak frequency and a peak frequency off the considered wave spectrum and also validates the initial assumptions. With the selected AFOSP FOWT, coupled aero-servo-hydro-elastic simulations have been performed for metocean data of a selected North Sea site with relatively severe conditions. For AFOSP, coupled models were set up in two aero-servo-hydro-elastic simulation codes of different levels of fidelity: for initial coupled analysis and to derive the distributed structural loads on the floating body the reduced d.f. nonlinear coupled multi-body FOWT model 'SLOW' (Simplified Low Order Wind turbine model), developed by the University of Stuttgart [34], is used, which is formulated in Newton–Eulerian equations of motion transformed into state-space. The nonlinear formulation of the coupled equations of motions in state-space is presented in equation (3.3). In equation (3.3), k is the vector of Corliolis, centrifugal and gyroscopic forces, p is the applied forces vector (gravitational forces, coupling forces between bodies, external forces equation (3.4)), M represents the mass matrix including added mass, x the model states and q the vector of the reduced models' d.f.

This coupled reduced model can resolve dynamics with low frequencies accurately up to the rotor frequency 1P, the frequency range containing most energy for wind turbines. All relevant external forces acting on the platform are summarized in equation (3.4), with the separate contributions represented in equations (3.5)–(3.7). The calculation of the hydrodynamic forces in horizontal direction F_{Morison} is based on Morison's equation (3.5), with effective spar diameter D_{eff} and height dz, water $u_{w,i}$, $a_{w,i}(t,z)$ and platform $u_{b,i}$, $a_{b,i}(t,z)$ velocity and acceleration over depth z. It is based on semi-empirical inertia, added mass and drag coefficients C_{M}, C_{A} and C_{D}, neglects diffraction effects [35] and includes the Froude–Krylov pressure along the water depth z applying the deepwater approximation depending only on the wave height η and the wavenumber k. The static pressure $p_{\mathrm{static}} = |\rho g z|$ on horizontal surfaces needs to be additionally accounted for when analysing internal stresses, otherwise it cancels out. The vertical hydrodynamic force acting in vertical direction on the spar's base at draft T (not including the hydrostatic contribution) is computed from the Froude–Krylov force F_{Krylov} and the radiation force from vertical platform motion (3.6). The mooring line forces are computed by using a force–displacement relationship (look-up table) derived from a quasi-static mooring model [36]. In the reduced model, the loads from aerodynamics are represented by an aerodynamic torque and the thrust force F_{aero} (3.7) on the shaft, being a function of only tip speed ratio TSR, rotor radius R, rotor azimuth angle θ and using the relative horizontal velocity of the rotor-plane v_{rel} to the incoming rotor-effective wind speed v_0 and c_{T} and c_{P}, the dimensionless thrust and power coefficients.

$$\dot{x} = \frac{\partial x}{\partial t}\begin{bmatrix}\dot{q}\\ \ddot{q}\end{bmatrix} = \begin{bmatrix}\dot{q}\\ M^{-1}(q(q,\dot{q},t) - k(q,\dot{q},t))\end{bmatrix} \tag{3.3}$$

$$F_{\mathrm{ext}} = (C_{\mathrm{hydrostatic}} + C_{\mathrm{Lines}}) \times q + F_{\mathrm{Morison}}(\dot{q},\ddot{q}) + F_{\mathrm{Krylov}}(q) + F_{\mathrm{aero}}(q,\dot{q}) \tag{3.4}$$

$$dF_{\mathrm{Morison}} = C_{\mathrm{M}} a_{w,i}(t,z) + C_{\mathrm{A}} a_{b,i} + C_{\mathrm{D}}(u_{w,i} - u_{b,i})|u_w - u_b|dz + \rho g D_{\mathrm{eff}} \eta e^{kz} dz, \tag{3.5}$$

$$F_{\mathrm{Krylov}} = \frac{\rho g D^2}{4}(\eta e^{kT}) \tag{3.6}$$

and

$$F_{\mathrm{aero}} = -\frac{1}{2}\rho\pi \begin{bmatrix} R^2 c_{\mathrm{T}}(\mathrm{TSR},\theta) \\ \dfrac{R^3 c_{\mathrm{P}}(\mathrm{TSR},\theta)}{\mathrm{TSR}} \end{bmatrix} v_{\mathrm{rel}}^2. \tag{3.7}$$

The advantage of this formulation compared to regular aero-servo-hydro-elastic models is that the nonlinear ordinary differential equation system only contains basic mathematic operations, no iterations or internal loops (as in blade element momentum aerodynamic models) and no

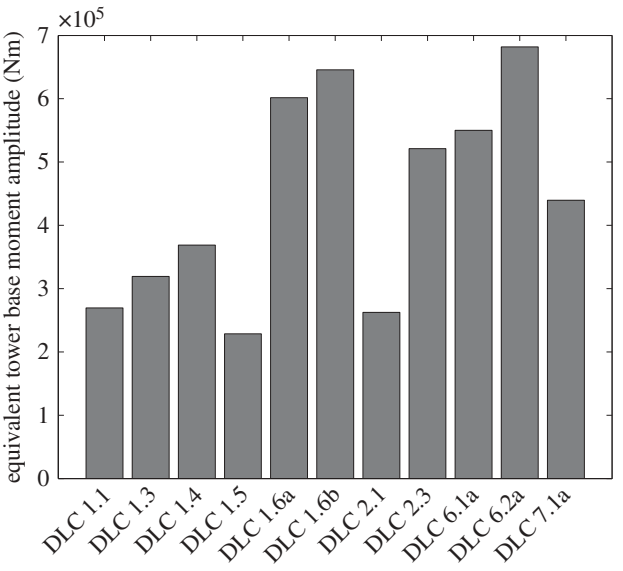

Figure 4. AFOSP DELs for different DLCs.

external preprocessing (as required for computing hydrodynamic coefficients). Only two one-dimensional external disturbances, wind and waves, are used as external inputs. Therefore, it can be used efficiently in optimization algorithms (figure 1) and also applied in linearized form for controller design [16].

Additional analyses with the NREL FAST code of a more comprehensive DLC set according to the International Electrotechnical Commission's standard IEC 61400-3 were performed to identify ultimate and fatigue loads. FAST accounts for turbulent wind inflow and computes the aerodynamic loading by a blade/element momentum-based approach including correction models to account for unsteady and wake effects. The hydrodynamics on the platform are simulated by a method based on first order potential flow theory and viscous effects accounting for wave radiation and diffraction effects. The mooring system is modelled in a quasi-static manner.

Figures 4 and 5 present the resulting AFOSP ultimate and fatigue loads computed with FAST at the critical tower base section for a selection of calculated IEC 61400-3 DLCs, with 1 representing power production; 2, power production plus occurrence of fault; 6, parked and 7, parked and fault conditions. The DELs have been calculated for each DLC applying the rainflow method, assuming a reference number of cycles $N_R = 2 \times 10^6$ and a probability distribution according to Rayleigh with the shape factor $k = 2$. The presented DELs are only shown for comparative analysis to the ultimate loads. In the actual fatigue analysis performed for AFOSP according to IEC only DLC 1.2, 2.4, 3.1, 4.1, 6.4, 7.2 and 8.3 were considered with their associated probability of occurrence for the FLS estimation where the main contribution (assuming availability greater than 90%) to fatigue damage is from the normal power production DLC 1.2 (equivalent to DLC 1.1). The most sensitive section of the whole monolithic concrete spar structure to fatigue loads was determined as the tower base section, where although the absolute internal forces are not the largest ones in the structure, its low diameter to minimize the wave loads yields the largest peak stresses of all sections. For the tower base extreme loads, figure 5 implies that the AFOSP structure is primarily dominated by the extreme wave conditions present in DLC 1.6 and 6.2 yielding the highest loads and exceeding the normal production load case DLC 1.1 loads by almost a factor of 2. For AFOSP, this high ratio is caused by the chosen extreme North Sea site with $H_s = 1.09$ and $H_{s,50} = 15.05$ m.

Based on the obtained loads and stresses, a structural analysis was performed to determine concrete thicknesses, amount of active and passive steel reinforcements and minimum

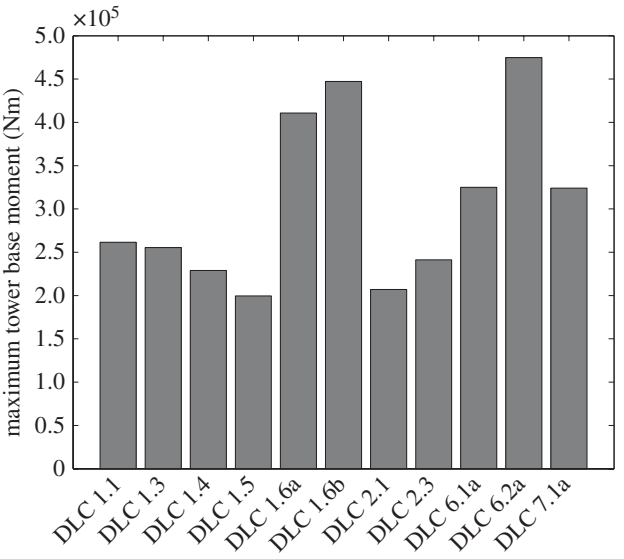

Figure 5. AFOSP Extreme loads for different DLCs.

pre-stressing forces that need to be applied in order to assure a compression state in each section under the maximum applied load. A FLS assessment following DNV-OS-J101 has been performed which determined the expected lifetime of the platform at 50 years.

For the AFOSP design, the coupled analysis of the DLC simulations with FAST identified the yaw degree of freedom to be particularly critical owing to the large structural inertia of the concrete design and low yaw stiffness and damping typical for cylindrical spars. Large yaw motions were present in DLCs with yawed wind inflow. To mitigate the yaw loads, the initial mooring line design was modified to increase the yaw stiffness considerably by a delta connection and increased line tension. Also a feedback control algorithm to suppress particularly excessive yaw motions during operation was developed. In parallel to the just presented numerical analyses, the experimental testing was performed. The next section presents first the general FOWT testing approach and then the specific procedure applied for AFOSP.

4. Experimental floating offshore wind turbine testing

Experimental testing of FOWT is usually performed to validate the numerical models, adjust viscous drag and damping parameters and obtain system dynamics in terms of RAOs. Tests are also used to investigate the performance in regular and irregular sea states, as well as under tow-out conditions and to test marine operations during installation and maintenance, which are difficult to model numerically. A typical test matrix therefore contains system identification cases (i.e. free decay, white noise wave, fixed displacement and mooring line force identification cases) and deterministic and stochastic separate and combined wind and wave cases.

The particular challenge of FOWT experimental testing is due to the fact that the system dynamics are governed by both aero- and hydrodynamic loads which are dominated by different physical properties. To ensure similitude of platform hydrodynamics, the platform properties are typically scaled by the dimensionless Froude number (4.1). It describes the ratio of inertial forces to gravitational forces in a fluid, assuming that the influence of viscous effects present in the thin boundary layer is small compared with the dominant factors gravity and inertia. The similitude of the incompressible aerodynamic flow over the wind turbine rotor is conserved by scaling according to the Reynolds number (4.2), defined as the ratio of inertial forces to viscous forces in a flow. The assumption of incompressible flow is valid, as the Mach number (4.7) for WT is typically

Table 1. Important dimensionless numbers for FOWT testing.

$Fr = \frac{v}{\sqrt{gl}}$ (4.1)	$Re = \frac{\rho l v}{\mu}$ (4.2)	$\mathrm{TSR} = \frac{\Omega R}{v}$ (4.3)	$\mathrm{KC} = \frac{v_m T}{l}$ (4.4)
$Ch = \frac{\rho v^2}{E_m}$ (4.5)	$\gamma = \frac{\rho a c R^4}{I_b}$ (4.6)	$Ma = \frac{v}{c_s}$ (4.7)	$St = \frac{fl}{v}$ (4.8)

well below 0.3. Froude scaling the structural stiffness may be omitted for parts of the tested system and the platform can be built rigid if the relation between the frequency f_{ext} of external forcing and the natural frequency f_n of structural vibration is small ($f_{ext} \ll f_n$). Otherwise, its influence is non-negligible. Particularly, the tower elasticity can have a large influence on RAOs, e.g. on TLPs [37].

Apart from the Froude and Re numbers, further properties may also become relevant, depending on the purpose of the experimental test. To preserve similarity in scaling of a wind turbine system behaviour, maintaining the tip speed ratio (4.3) is a key factor, which is the ratio of the rotor's velocity to the wind's free stream velocity. A constant TSR constrains rotational frequencies and wind speed and is compatible with Froude scaling. If applying Froude scaling, it is important to also observe the value of the Keulegan–Carpenter number (4.4), which is characteristic for planar oscillating flows. A small KC number indicates that viscous effects in terms of flow separation can be neglected. For correct aeroelastic preservation and establishing consistency of loads and stability of a rotor system, the Lock number (4.6) is important which is defined as the ratio of aerodynamic to inertial forces in rotor blades and is often used for helicopter rotor testing. Lock number scaling ensures that the rotor has the correct aerodynamic damping and aerodynamic coupling characteristics and is useful for modelling rotor performance coefficients and structural loadings especially in unsteady conditions, i.e. wind-wave loading. If VIV-driven effects are relevant, conservation of the Strouhal number (4.8), a dimensionless number describing oscillating flows, is recommended. If Froude scaling is used, the Strouhal number cannot always be maintained because of its dependence on phenomena characterized by different Reynolds number regimes. However, the Strouhal number stays at a value of 0.2 for a range of Reynolds numbers and its effects have been neglected in past experiments. In dedicated mooring line testing, the Cauchy number (4.5) is important, which is defined as the ratio of inertial forces to elastic forces in a mooring line. Generally, it is completely compatible with Froude scaling. Froude scaling the modulus of elasticity of a mooring line yields equality in the Cauchy number between full and model scales if the model and test scale mooring lines have the same density, which may be an issue. The Weber number which measures the balance of hydrodynamic surface tension to inertial loads is not expected to have importance, except at very small scales. In table 1, v and v_m denotes the fluid and maximum fluid velocity; l, the characteristic length (for a spar the cylinder diameter); ρ, the fluid density; μ, its dynamic viscosity; Ω, the rotor speed; R, the rotor radius; T, the fluid oscillation period; E_m, the bulk modulus of elasticity; I_b, the moment of inertia of a rotor blade; c, the blade chord length; a, the aerofoil lift slope; c_s, the speed of sound and f, the frequency of shed vortices.

The main issue arising for FOWT testing in combined wind and wave basins is that hydrodynamic and aerodynamic similitude according to Froude and Reynolds scaling can practically not be achieved. Currently, the most popular solutions for the concurrent aero- and hydrodynamic scaling law dilemma present in combined FOWT wind and wave tests is based on Froude scaling. The method preserves the hydrodynamic wave force acting on the platform and ensures that the global FOWT rigid-body motion is similar to the full scale system by preserving the ratio of inertial, aero- and hydrodynamic and mooring line loading and by scaling consistently the load, structural and rotor frequencies, implying that the tip speed ratio and KC number are also scaled correctly. The difference in water density between fresh water and seawater, as

well as air density deviations in the experiment are also accounted for if relevant. The practical scaling procedure is that the geometric length, time, mass (mass, moment of inertia), structural stiffness (yielding correct structural natural frequency, gyroscopic moment) and environmental properties (wind, wave velocity) of the FOWT system are scaled according to Froude. By applying this scaling to the full-scale rotor blade geometry, the resulting thrust force (dominating the FOWT system global motion and loading during wind turbine operation) is not scaled correctly because the rotor aerodynamics are governed by the Reynolds number which is then lower in model scale resulting in reduced lift-over drag ratios C_l/C_d of the aerofoils. Owing to this Reynolds number dependency, a geometrically scaled rotor would need to operate at very high angles of attack in the proximity of stall to achieve the correct thrust force, resulting in wrong aerodynamic damping (the derivative of C_l with respect to the angle of attack is mainly governing aerodynamic damping) and unsteady aerodynamic effects close to stall, that are difficult to predict.

To overcome that issue, the scaled rotor blades are redesigned with low-Reynolds number aerofoils (to avoid drastic changes in lift and drag coefficients caused by small inflow irregularities and still provide sufficient lift) operating at their optimal lift-over drag ratio at angles of attack far away from the stall region, but subsequently relatively low lift coefficients compared with the full scale aerofoils operating at high Reynolds numbers. To still achieve the Froude-scaled thrust coefficient of the scaled rotor the chord length is increased. This technique leads to axial induction factors of the rotor close to the Betz optimum and preserves the thrust similitude correctly, but the aerodynamic and generator torque and power as well as the flow around the blades are not scaled correctly, leading to dissimilarities in the platform roll loads and differences in the 3P excitation of the blade passing the tower. Apart from compensating the incorrect aerodynamic Reynolds number, the scaling method leads to an incorrect aerodynamic Mach number and aerodynamic Strouhal number which can be neglected. The hydrodynamic Reynolds number mismatch and incorrect viscous wave and form drag may be compensated by applying frictional drag extrapolation techniques from model to full scale, e.g. following ITTC recommendations. The scaling also leads to low wind velocities in the experiment, which may render it difficult to ensure a controlled, constant wind inflow velocity and turbulence level because of flow perturbations from heat convection and limitations of the wind generators. An approach developed by Bredmose & Müller [38] is to introduce a free parameter β where $\beta = 1$ is equivalent to Froude scaling, while $\beta < 1$ implies larger air velocities than for Froude scaling.

The approach of a redesigned rotor at model scale is able to deliver the correct thrust thus representing a valid wind-wave tank testing methodology, e.g. [39–43]. Furthermore, given that the mass distribution and rotational speed are scaled correctly, the correct gyroscopic forces and 1P, 3P forcing frequencies will be reproduced [44,45]. If also the structural stiffness is scaled correctly, the structural frequencies and deflection to the loads will scale correctly [44,45], as well as the interaction of the mooring dynamics with the global response of the FOWT [46]. In case the focus of the test is on the aerodynamic performance of the turbine under consideration of the platform motions, wind tunnel testing of a turbine may be performed with the platform motions prescribed by an actuator controlled in real time by a hydrodynamic software representing the scaled platform [47–49]. A broad overview of the scaled FOWT tests performed so far can be found in Müller *et al*. [38].

5. AFOSP experimental campaign and results

Particularly during early pre-design of a FOWT, the outlined Froude scaling approach may be unnecessarily complex and cost-intensive, as it requires a wind turbine model with redesigned blades and access to a large combined wind and wave basin. Owing to the fact that typically an existing wind turbine is chosen for a developed floating substructure, the focus of the early experiments can be placed on identification of global system behaviour in terms of platform eigenfrequencies, RAOs and tower base loads as well as tower top displacements and accelerations during typical operational and extreme load cases. To establish these quantities, the

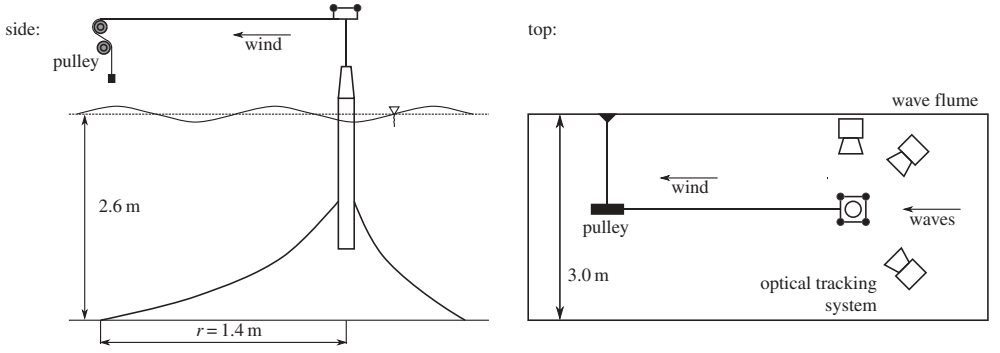

Figure 6. Experimental set-up for the AFOSP platform in the CIEM wave flume.

rotor thrust force may be modelled by simpler approaches ranging from concentrated masses with added point forces [50], drag discs with a rotating body [4] to real-time controlled thrust actuators (so-called Software in the loop SIL approaches) [51,52].

(a) AFOSP experimental set-up

The RAO and wind/wave tests for AFOSP were performed at the CIEM (Canal d'Investigació i Experimentació Marítima) wave flume at the Lab of Marine Engineering at the Universitat Politècnica de Catalunya, which is 100 m long, 3 m wide and up to 7 m deep. Figure 6 shows a descriptive diagram of the experimental set-up. For the free decay tests, a wave basin without a wave making device at the same location was used with a width of 4.6 m, length of 10 m and water depth of 2.6 m. Its larger width compared with the wave flume mitigated the effect of wave refraction. Based on the wave flume dimensions, the scale of the system was defined as 1 : 100, which is about two to three times smaller in scale than most other FOWT wind/wave tests. The larger scales are usually applied to avoid the previously explained aerodynamic scaling issues of the rotor owing to small Reynolds numbers. Platform motions and accelerations were measured by both inertial sensors (triaxial accelerometer, triaxial gyro, 128 Hz sampling rate) and by a 6 d.f. optical tracking system capable of computing the three-dimensional coordinates of the selected points placed at the tower top with an accuracy of approximately 1 mm at 120 Hz sampling rate. Additionally, the wind device was monitored with a rotational transducer measuring the angular rotation of the pulley and the mooring tension with a tension gauge at the anchor location. The full-scale platform design corresponding to the experimentally tested scaled spar had an approximate total mass (including ballast) of 17 000 metric tons, a draft of 130 m and a base cylinder diameter of 13 m.

In the wave flume, no wind generating fans could be used for the experiment [22], so another simplified method is applied to still model the static mean thrust force. The wind force is applied by a mechanical pulley system, composed of two nylon pulleys and a weight tied to a wire that acts at the top of the platform, as depicted in figure 6. The selected pulleys have almost negligible mass and inertia in order to avoid dynamic damping and other interferences and the nylon rope's density is small enough to avoid slacks and thus temporal variation of the force and damping while the platform oscillates. With the assumption that the pulley wheel is always oriented in the vertical plane through the wire, and assuming that the wheel runs without any friction, the equation for the force F_p applied at the scaled model tower top can be computed by equation (5.1) with m as pulling mass; A, denoting the acceleration vector at the connection to the platform tower top; I_{zz}, the rotational inertia of the pulley wheel; R_p, its radius and e_2, the normalized vector in the pulling wire's direction. The mass is selected to provide the Froude-scaled mean thrust force

at the chosen wind conditions.

$$F_{\mathrm{p}} = \left(m(g + A \cdot e_2) + \frac{I_{zz} A \cdot e_2}{R_{\mathrm{p}}^2} \right) e_2. \tag{5.1}$$

A truncated catenary system including two segments with different weight, a lighter chain on the suspended stretch and a heavier chain towards the anchor, has been designed to fit the stiffness of the scaled mooring system, whose scaled radius was exceeding the width of the used wave flume. The quasi-static force–displacement stiffness relationship characteristics of this system were validated by a test in dry conditions of the lines connected to a fixed steel frame and movable fairlead connections, so that discrete positions of the platform could be in the SWL plane and the resulting tension measured. Based on these measurements and required basic input such as length, mass and submerged weight, a quasi-static mooring line model was developed to fit the experimental data. In addition, the geometric and material properties of the two scaled chains' links were measured and based on the data a CAD model was set up to compute not easily measurable properties required for the dynamic mooring line model such as the chains' inertias.

The performed AFOSP 2014 test campaign consisted of initial calibration tests for the camera 3D tracking of platform motions and inertial sensors, experimental identification of the platform mass properties, water tightness checks, hydrostatic free decay tests of the platform in a water basin with and without wind and mooring system and the hydrodynamic tests in the wave flume. The hydrodynamic tests were used to validate RAOs, investigate extreme wave conditions with a parked turbine and analyse the system's operational and extreme behaviour under combined wind and wave loading.

(b) Comparison with numerical simulation

In the case of AFOSP, particularly owing to the uncommon wind forcing device used, the results of the experiment were not only upscaled and compared with the full-scale aero-servo-hydro-elastic simulation results but also a dedicated numerical model was set up to be directly compared with the experiment. This dedicated scaled model was set up using the multi-purpose flexible multi-body software SIMPACK. The SIMPACK code's capabilities for dynamic floating offshore wind turbine simulation have been verified by code-to-code comparisons during the IEA Wind tasks 23 and 30 (OC3 and OC4 projects).

Using Froude-scaled hydrodynamic coefficients, the hydrodynamic linear potential flow module HydroDyn (NREL) coupled to SIMPACK, accounting for radiation and diffraction forces, was applied to compute the hydrodynamic forces. For the force of the pulley acting at the top of the tower equation (5.1) was implemented. For modelling of the segmented truncated mooring system, initially the quasi-static model validated in the dry-condition tests was used. Also an in-house nonlinear dynamic multi-body mooring line model [53] was used to check the applicability of the quasi-static approach that is modelled in the same multi-body environment (SIMPACK) as the platform. The structurally very stiff scaled AFOSP platform and tower were modelled as rigid bodies. Note that the dedicated SIMPACK model used for the comparison with the experimental data is different from the simplified coupled nonlinear multi-body model SLOW outlined in equations (3.3)–(3.7).

First, the free decay tests were compared to tune the additional added mass, inertia and damping values. As initial values for the simulation, values were obtained from a simple nonlinear system for the roll/pitch and heave motions according to equation (5.2), based on [54]. The nonlinear term is linearized by a Fourier series expansion (5.3) to obtain the linearized equation of motion (5.4). The general form of the solution for can be expressed as (5.5) and (5.6)

$$(M + M_{\mathrm{a}})\ddot{x} + b_1\dot{x} + b_2|\dot{x}|\dot{x} + Kx = 0, \tag{5.2}$$

$$|\dot{x}|\dot{x} = \frac{8}{3\pi}\omega_0 x_k x, \tag{5.3}$$

$$(M + M_a)\ddot{x} + \left(b_1 + \frac{8b_2}{3\pi}\omega_0 x_k\right)\dot{x} + Kx = 0, \tag{5.4}$$

$$x = x_0 e^{-\zeta w_0 t} \sin\left(\sqrt{1-\zeta^2} w_0 t + \varepsilon\right), \tag{5.5}$$

$$\zeta = \frac{C}{2(M + M_a)w_0}, \tag{5.6}$$

$$\delta = \ln\left(\frac{x_k}{x_{k-1}}\right), \tag{5.7}$$

$$\delta = 2\pi\zeta, \tag{5.8}$$

and

$$Y = \frac{1}{2\pi}\ln\left(\frac{x_k}{x_{k-1}}\right) = \frac{b_1}{2(M + M_a)w_0} + \frac{4b_2}{3\pi(M + M_a)}x_k, \tag{5.9}$$

where ζ is the damping ratio; δ, the logarithmic decrement (5.7); ε, the phase angle; w_0, the damped natural frequency and x_0 and x_k, the initial amplitude and amplitude of the k-th oscillation, respectively. The added mass M_a and inertia I_a can be estimated from the measured frequency w_0 and the known hydrostatic stiffness $C_{hydrostatic}$. Assuming small values of ζ (5.8), a linear relationship can be established (5.9) where the linear and quadratic damping b_1, b_2 can be derived based on the measured decrement and damped natural frequency and using linear regression.

Using these estimated damping values, simulations of the free decay tests at model scale were performed. In figure 7, the comparison for the pitch/roll free decay case without mooring system is presented. The simulated results and the experimental data match well in terms of the magnitude of the power spectral density (PSD) peak, its frequency and damping ratio. Regarding the damping, the numerical simulation for the first 8 periods matches the experimental data very well, but for the following periods the simulation shows further decreasing amplitudes, while the experimental data amplitudes decrease much slower and for some subsequent cycles (e.g. periods 11–12) have the same magnitude. Main reason for the deviation is that starting with the 8th period the waves radiated from the platform during its pitch motion and refracted from the water basin walls interact with the platform and add energy back into the system. While the damping values b_1, b_2 derived with equation (5.9) for heave and yaw can directly be used in the simulation, the derived damping $b_{1,2}$ for pitch/roll and surge/sway needs to be adjusted because the frequency-dependent linear hydrodynamic radiation damping B is nonzero for these d.f. and therefore already accounted for in the simulation. A practical approach is to use equation (5.9) and derive only the linear damping b_1 by setting $b_2 = 0$ before the fit and then subtracting B to estimate the damping used in the simulation: $b_1^* = b_1 - B$. The results validate the selection of the additional added mass/inertia and damping in pitch direction, as well as the correct scaling of the hydrostatic matrix. If in the simulation the linear hydrodynamic forces are supplemented by the viscous drag term in Morison's equation, an appropriate value for C_D needs to be derived. A practical approach is to start by using literature values like $C_D = 1.0$ and then adjusting the additional damping b_1, b_2 and C_D to match the experimental data. For AFOSP, the latter approach with $C_D \neq 0$ was used to ensure that in cases with waves their drag force is accounted for.

In figure 8, the yaw-free decay case with mooring is depicted. Here the dynamic multi-body mooring system was also used to verify the derived additional inertia in yaw from the experiments. Both simulations with quasi-static and dynamic mooring system model show very similar results, confirming the low influence of mooring line dynamics in the case of AFOSP. The simulations also match the experiment well and hereby verify both numerical mooring line models. Owing to the significant additional computational effort required for the dynamic mooring line model and its low influence on results, the quasi-static model was used in all subsequent simulations. Overall, the free decay tests were very valuable to adjust the damping and added mass/inertia terms for the simulations and for all d.f. maximum deviation of less than or equal to 2% could be achieved for both the logarithmic decrements and eigenfrequencies.

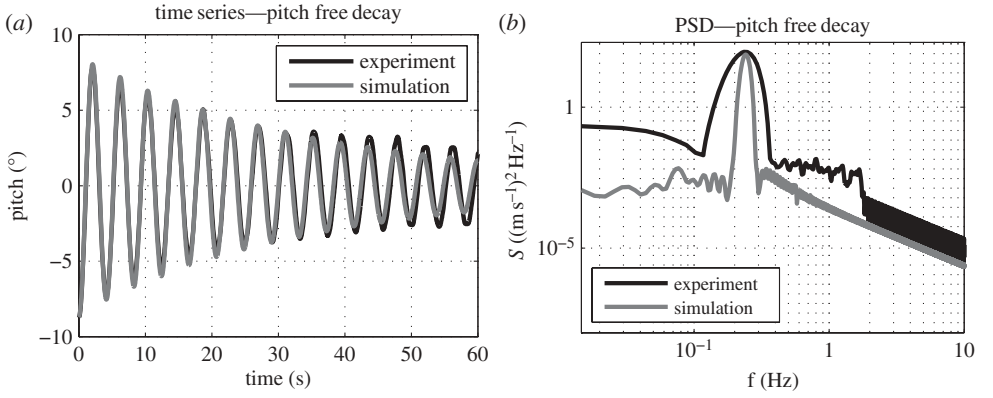

Figure 7. Pitch free decay without mooring system: (*a*) time series and (*b*) PSD.

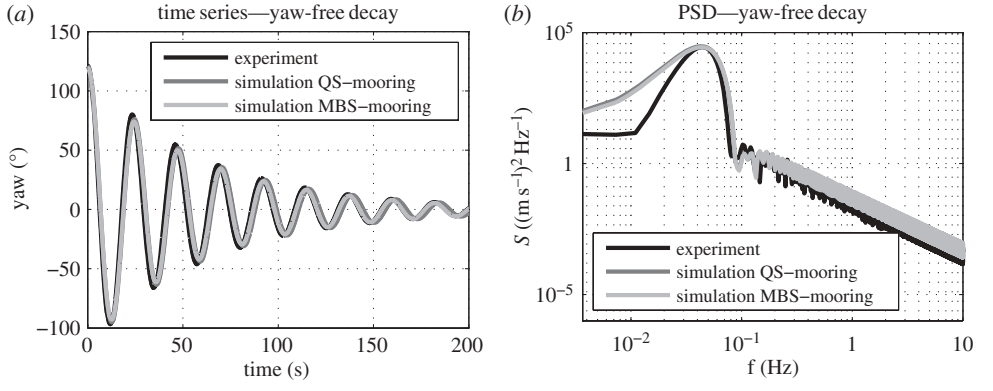

Figure 8. Yaw-free decay with mooring system: (*a*) time series and (*b*) PSD.

The next phase of experiments was used to identify the RAOs of the AFOSP platform experiments with regular waves with periods ranging from 0.8 to 4.8 s, in 0.2 s steps. To derive the RAOs, the time series were analysed by extracting the average amplitudes for all six platform d.f. and normalizing them by the corresponding wave amplitudes. Present transients in the simulation, as well as during the experiments were excluded. Figure 9 presents the RAOs from both experiment and simulation for platform surge and pitch. The results agree very well in terms of maximum amplitude and wave period, also for heave which is not shown. The RAOs for the other d.f. sway, roll and yaw were not measured, because in the experiment the waves were always directed in one direction along the wave flume and the platform and mooring system were not rotated. Although owing to the symmetry of the platform, sway and roll RAOs also are expected to match, and the correct yaw behaviour which is not excited significantly by waves at any incident-direction could already be validated by the yaw-free decay test. Figure 9 illustrates, that in the proximity of the peak RAO, the magnitude changes with a very high gradient so that additional tests, respectively simulations, could be beneficial to more exactly identify the RAO peak frequency and magnitude for each d.f. Based on the successful adjustment of the damping coefficients during the free decay tests, these tests were assumed to be not required.

The purpose of the combined wind and wave tests is primarily to check the FOWT behaviour in extreme conditions in terms of maximum inclination angles and maximum nacelle accelerations. The comparison to the simulated AFOSP results was also used to validate the correct modelling of the experimental pulley (equation (3.4)), in particular to verify the

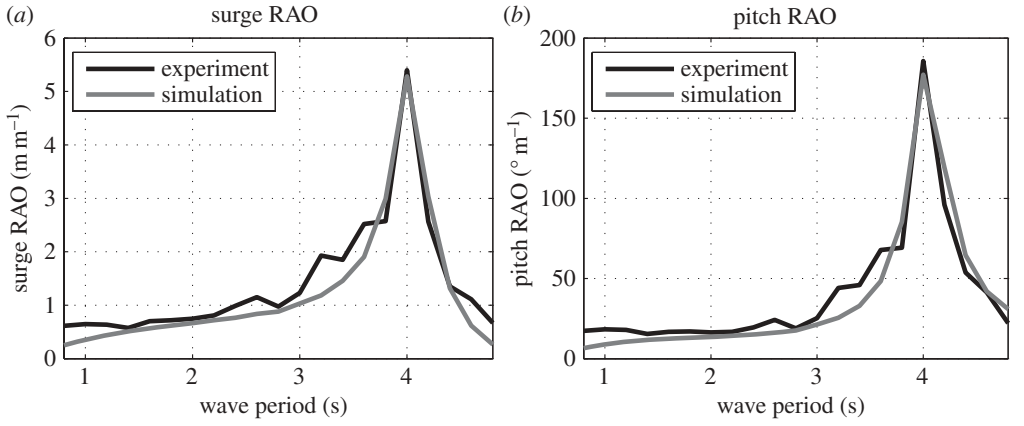

Figure 9. RAOs for platform (*a*) surge and (*b*) pitch.

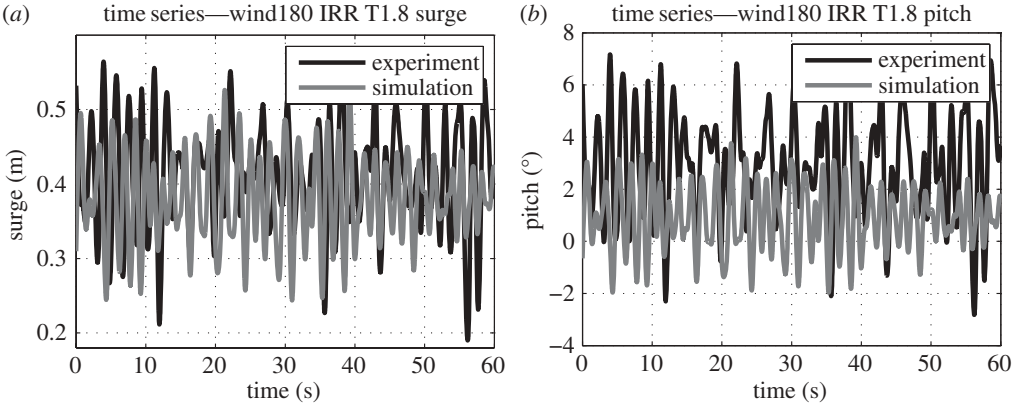

Figure 10. Wind–Wave case; set-up: irregular waves at ($T = 1.8$ s, $H = 21.4$ cm) with mooring system; quantities: surge d.f. time series (*a*) and PSDs (*b*).

assumption of the frictionless pulley wheel and that the wire attached to the turbine does not slip on the pulley wheels. The free decay and RAO tests were performed with no waves or regular Airy waves and no wind force applied at the nacelle. Therefore, only 3 d.f. were excited at the same time. The Wind and Waves test features cases with irregular waves and a misaligned wind force applied at the nacelle. Figure 10 presents an exemplary result for one extreme case, with irregular waves at $T = 1.8$ s, a wave height of $H = 21.4$ cm and maximum operational thrust force at the rotor. The results between experiment and simulation agree well for the presented surge d.f., both in the frequency domain in terms of the two peaks associated with wave frequency and surge natural period and time series in terms of mean value and amplitude. This case under severe wind and wave conditions, which are beyond the operational envelope, confirms the accurate performance and load predictions of the numerical simulations under complex loading conditions where more than 3 d.f. are excited and where moorings, hydrodynamics and aerodynamics interact.

Clearly, the mechanical pulley system is limited in its application, because it does not consider rotor dynamic effects such as gyroscopic loads and elastic effects, any transient aerodynamic effects such as aerodynamic damping and control related effects. This means that instabilities or dynamically amplified loads owing to aerodynamic and aeroelastic coupling effects may not be identified. Another limitation of the pulley is related to the dynamics of the pulley system.

The inertial forces experienced by the suspended mass, the inertia of the nylon pulley and the static and dynamic frictional moments of the bearing lead to non-negligible oscillations of the force around the average value depending on the floating platform accelerations at the nacelle. However, the platform behaviour in waves is represented in a more realistic way with the pulley system, because the platform has the correct mean pitch heel angle and surge displacement leading to correct mean mooring line tensions. Additionally, comparisons with FAST simulations corresponding to the same wind and wave conditions have shown that the obtained platform motions with the pulley system tend to yield conservative results. A main reason for that result is that the pulley neglects the favourable aerodynamic damping.

6. Conclusion

A general pre-design process of a FOWT was presented and the application of the procedure was illustrated for the AFOSP monolithic concrete spar buoy design. The AFOSP experimental campaign performed during the pre-design stage was sufficient to provide vital information for the subsequent detailed design and concept industrialization

- adjustment and validation of hydrodynamic and viscous damping coefficients for linear potential flow hydrodynamic models, as well as reduced Morison-based models;
- validation of platform natural frequencies, i.e. platform behaviour in still water;
- validation of RAOs, i.e. platform behaviour in waves;
- evaluation of basic load statistics, dynamic accelerations, heel angle for platform and RNA for extreme conditions accounting at maximum rotor thrust and in severe sea state conditions; and
- general concept viability check, i.e. ensuring that no severe design errors are present in the pre-design.

The known limitations of this simplified experimental campaign are that instabilities or resonances can be identified only to a very limited extent because, if present, are likely caused by unexpected aero-hydro-servo-elastic coupling effects. Such effects may also not be captured by the applied reduced nonlinear numerical models. Yet during the early design stage of a FOWT, the obtained information about system natural frequencies, RAOs, mooring line tensions, dynamic behaviour in irregular waves and displacements, accelerations and loads under a mean wind thrust may already provide all necessary information to take a qualified decision to proceed with the chosen design into the detailed design stage. The pre-design test campaign also ensures that the methodologies and numerical tools used are sufficient to accurately to model the coupled dynamics of the specific system. After a refined detailed design is defined and the required DLC simulations are performed and analysed in terms of extreme and fatigue loads, only selected critical DLC (including installation and marine operations) may be required to be experimentally tested in a wind/wave facility with a more sophisticated FOWT model at a larger scale. This two-staged testing procedure is deemed to be more efficient than to perform sophisticated experiments already at an early design stage.

Funding statement. The research presented on the AFOSP design experiments and numerical calculations was performed during the KIC-InnoEnergy project AFOSP, funded by the European Institute of Innovation and Technology (EIT). The research on FOWT design procedures and on experimental procedures has also received funding from the European Community's Seventh Framework Programme FP7-ENERGY-2012-1-2STAGE under grant agreement no. 308 974(INNWIND.EU).

References

1. Nielsen FG, Hanson TD, Skaare B. 2006 Integrated dynamic analysis of floating offshore wind turbines. In *Proceedings of ASME 2006 25th International Conference on Offshore Mechanics and Arctic Engineering* (*OMAE 2006*), *Hamburg, Germany, 4–9 June 2006*, pp. 681–689. New York, NY: American Society of Mechanical Engineers.

2. Myhr A, Maus KJ, Nygaard TA. 2011 Experimental and computational comparisons of the OC3-HYWIND and Tension-Leg-Buoy (TLB) floating wind turbine conceptual designs. In *Proceedings of the Twenty-first (2011) International Offshore and Polar Engineering Conference (ISOPE 2011), 8, Maui, USA, 19–24 June 2011*, pp. 353–360. Mountain View, CA: International Society of Offshore and Polar Engineers.
3. Roddier D. 2009 WindFloat: a floating foundation for offshore wind turbines part I: design basis and qualification process. In *Proceedings of ASME 2009 28th International Conference on Ocean, Offshore and Arctic Engineering (OMAE 2009), Honolulu, USA, 31 May–5 June 2009*, pp. 845–853. New York, NY: American Society of Mechanical Engineers.
4. Cermelli C, Roddier D, Aubault A. 2009 WindFloat: a floating foundation for offshore wind turbines II. Hydrodynamics analysis. In *Proceedings of ASME 2009 28th International Conference on Ocean, Offshore and Arctic Engineering (OMAE 2009), Honolulu, USA, 31 May– 5 June 2009*, pp. 135–143. New York, NY: American Society of Mechanical Engineers.
5. Aubault A, Cermelli C, Roddier D. 2007 Parametric optimization of a semi-submersible platform with heave plates. In *Proceedings of ASME 2007 26th International Conference on Offshore Mechanics and Arctic Engineering (OMAE 2007), San Diego, USA, 10–15 June 2007*, pp. 471–478. New York, NY: American Society of Mechanical Engineers.
6. Roddier D, Cermelli C, Aubault A, Weinstein A. 2010 WindFloat: a floating foundation for offshore wind turbines. *J. Renew. Sust. Energy* **2**, 033104. (doi:10.1063/1.3435339)
7. Fukushima Offshore Wind Consortium. 2014 Fukushima floating offshore wind farm demonstration project (Fukushima FORWARD). See http://www.fukushima-forward.jp/pdf/pamphlet3.pdf abgerufen
8. Arapogianni A, Genach A-B. 2013 *Deep water—the next step for offshore wind energy*. Technical Report. Brussels, Belgium: European Wind Energy Association (EWEA).
9. Henderson AR, Witcher D. 2010 Floating offshore wind energy—a review of the current status and an assessment of the prospects. *Wind Eng.* **34**, 1–16. (doi:10.1260/0309-524X.34.1.1)
10. Consulting Main(e) International, LLC. 2013 *Floating Offshore Wind Foundations: Industry Consortia and Projects in the United States, Europe and Japan—an overview.* Report, Bremen, USA. Q3
11. Wang CM, Utsunomiya T, Wee SC, Choo YS. 2010 Research on floating wind turbines: a literature survey. *IES J. A* **3**, 267–277. (doi:10.1080/19373260.2010.517395)
12. IEC 61400-1, Ed. 3. 2005 *Wind turbines—part 1: design requirements*. International Electrotechnical Commission (IEC). Q4
13. DNV-OS-J103. 2013 *Design of floating wind turbine structures*. Offshore Standard, Det Norske Veritas (DNV). Q4
14. IEC 61400-3, Ed. 1. 2009 *Wind turbines—part 3: design requirements for offshore wind turbines*. International Standard, International Electrotechnical Commission (IEC).
15. Kvittem MI, Bachynski E, Moan T. 2012 Effects of hydrodynamic modelling in fully coupled simulations of a semi-submersible wind turbine. *Energy Proc.* **24**, 351–362. (doi:10.1016/j.egypro.2012.06.118)
16. Sandner F, Schlipf D, Matha D, Cheng PW. 2014 Integrated optimization of floating wind turbine systems. In *Proceedings of the ASME 2014 33rd International Conference on Ocean, Offshore and Arctic Engineering (OMAE 2014), San Francisco, USA, 8–13 June 2014*, p. V09BT09A030. New York, NY: American Society of Mechanical Engineers.
17. Skaare B, Hanson TD, Nielsen FG, Yttervik R, Hansen AM, Thomsen K, Larsen TJ. 2007 Integrated dynamic analysis of floating offshore wind turbines. In *Proceeding of European Wind Energy Conference and Exhibition (EWEC 2007) (S. 1929–1939), Milan, Italy, 7–10 May 2007*. Brussels, Belgium: European Wind Energy Association.
18. Härer A, Matha D, Kucher D, Sandner F. 2013 Optimization of offshore wind turbine components in multi-body simulations for cost and load reduction. In *Proceedings of the EWEA Offshore, Frankfurt, Germany, 19–21 November 2013*. Brussels, Belgium: European Wind Energy Association.
19. Fernandez J, Laidler A, Izarra J, Innovation M, Murueta D, Malloape B. 2013 Design considerations of a semisubmersible platform for offshore wind turbines. In *Proceedings of the EWEA Offshore, Frankfurt, Germany, 19–21 November 2013*. Brussels, Belgium: European Wind Energy Association.
20. Huijs F, Mikx J, Savenije F, Ridder E-JD. 2013 Integrated design of floater, mooring and control system for a semi-submersible floating wind turbine. In *Proceedings of the EWEA Offshore, Frankfurt, Germany, 19–21 November 2013*. Brussels, Belgium: European Wind Energy Association.

21. Hong S, Kim J, Hong S, Kim H. 2012 Design and analysis of a box floater with damping plates for floating wind turbine platform. In *The Proceedings of The Twenty-second (2012) International Offshore and Polar Engineering Conference* (*ISOPE 2012*), *4, Rhodes, Greece, 17–23 June 2012*, pp. 411–416. Mountain View, CA: International Society of Offshore and Polar Engineers.
22. Molins C, Campos A, Sandner F, Matha D. 2014 Monolithic concrete off-shore floating structure for wind turbines. In *Proceedings of the EWEA 2014 Annual Event, Barcelona, Spain, 10–13 March 2014*. Brussels, Belgium: European Wind Energy Association.
23. Iijima K, Kawai M, Nihei Y, Murai M, Ikoma T. 2013 Conceptual design of a single-point-moored FOWT and tank test for its motion characteristics. In *Proceedings of the ASME 2013 32nd International Conference on Ocean, Offshore and Arctic Engineering* (*OMAE 2013*), *Nantes, France, 9–14 June 2013*, p. V008T09A079. New York, NY: American Society of Mechanical Engineers.
24. Copple RW, Capanoglu C. 2012 Tension leg wind turbine (TLWT) conceptual design suitable for a wide range of water depths. In *Proceedings of the Twenty-second* (*2012*) *International Offshore and Polar Engineering Conference* (*ISOPE 2012*), *4, Rhodes, Greece, 17–23 June 2012*, pp. 396–403. Mountain View, CA: International Society of Offshore and Polar Engineers.
25. Suzuki K, Yamaguchi H, Akase M, Imakita A, Ishihara T, Fukumoto Y, Oyama T. 2011 Initial design of tension leg platform for offshore wind farm. *J. Fluid Sci. Technol.* **6**, 372–381. (doi:10.1299/jfst.6.372)
26. Chakrabarti S. 2005 *Handbook of offshore engineering*, vol. 1, 1st edn. Plainfield, IL: Elsevier.
27. Molins C, Campos A, Matha D, Sandner F. 2014 *Estructura flotante para soporte de turbinas eólicas marinas y procedimiento para su construcción e instalación*. Patent no. P201430259.
28. Molins C, Rebollo J, Campos A. 2011 *Estructura flotante de hormigón prefabricado para soporte de aerogenerador*. Patent no. WO201393160.
29. Molins C, Rebollo J, Campos A. 2012 *Procedimiento de instalación y mantenimiento de estructura flotante monolítica para soporte de aerogenerador*. Patent no. WO2013117796.
30. Jonkman J, Butterfield S, Musial W, Scott G. 2009 *Definition of a 5MW Reference Wind Turbine for Offshore System Development.* Technical Report, NREL, Golden, CO: NREL (NREL/TP-500-38060).
31. McCormick ME. 2009 *Ocean engineering mechanics*, 1st edn. New York, NY: Cambridge University Press.
32. DNV-OS-J101. 2013 *Design of offshore wind turbines*. Offshore Standard, Det Norske Veritas (DNV).
33. Fossen TI. 2011 *Handbook of marine craft hydrodynamics and motion control*, 1st edn. Chichester, UK: John Wiley & Sons.
34. Sandner F, Schlipf D, Matha D, Seifried R, Cheng PW 2012 Reduced nonlinear model of a spar-mounted floating wind turbine. In *Proceedings of the German Wind Energy Conference* (*DEWEK 2012*), *Bremen, Germany, 7–8 November 2012*. Wilhelmshaven, Germany: Deutsches Windenergie-Institut. See http://elib.uni-stuttgart.de/opus/volltexte/2013/8439/pdf/Sandner_ReducedModel_Dewek2012.pdf.
35. Matha D, Sandner F, Schlipf D. 2012 Efficient critical design load case identification for floating offshore wind turbines with a reduced nonlinear model. In *Proceedings of the Science of Making Torque from Wind, Oldenburg, Germany, 9–11 October 2012*. Oldenburg, Germany: European Academy of Wind Energy.
36. Jonkman J. 2007 Dynamics Modeling and Loads Analysis of an Offshore Floating Wind Turbine. PhD dissertation, Golden, CO. (NREL/TP-500-41958).
37. Matha. 2009 *Model development and loads analysis of an offshore wind turbine on a tension leg platform, with a comparison to other floating turbine concepts*. Technical Report. Golden, CO. (NREL/TP-500-45891).
38. Müller K, Sandner F, Bredmose H, Azcona J, Manjock A, Pereira R. 2014 Improved tank test procedures for scaled floating offshore wind turbines. In *Proceedings of the International Wind Engineering Conference* (*IWEC 2014*) (*S. 1–12*), *Hannover, Germany, 3–4 September 2014*. Hannover, Germany: Leibniz Universität Hannover. See http://elib.uni-stuttgart.de/opus/volltexte/2014/9548/pdf/Mueller2014_Improved_Tank_Test_Procedures_For_Floating_Offshore_Wind_Turbines.pdf.
39. Kimball R, Goupee AJ, Fowler MJ, Ridder E-JD, Helder J. 2014 Wind/wave basin verification of a performance-matched scale-model wind turbine on a floating offshore wind turbine platform. In *Proceedings of the ASME 2014 33rd International Conference on Ocean, Offshore and*

Arctic Engineering (*OMAE 2014*), *San Francisco, USA, 8–13 June 2014*, p. V09BT09A025. New York, NY: American Society of Mechanical Engineers.

40. Martin HR, Kimball RW, Viselli AM, Goupee AJ. 2012 Methodology for wind/wave basin testing of floating offshore wind turbines. In *Proceedings of the ASME 2012 31st International Conference on Ocean, Offshore and Arctic Engineering* (*OMAE 2012*), *Rio de Janeiro, Brazil, 1–6 July 2012*, pp. 445–454. New York, NY: American Society of Mechanical Engineers.
41. Jain A, Robertson AN, Jonkman JM, Goupee AJ, Kimball RW, Swift AH. 2012 FAST code verification of scaling laws for DeepCwind floating wind system tests preprint Anant Jain. In *Proceedings of the Twenty-second* (*2012*) *International Conference on Offshore and Polar Engineering* (*ISOPE 2012*), *Rhodes, Greece, 17–23 June 2012*, pp. 355–365. Mountain View, CA: International Society of Offshore and Polar Engineers.
42. Martin HR. 2011 Development of a scale model wind turbine for testing of offshore floating wind turbine systems. PhD dissertation, University of Maine.
43. Fowler M, Iii DA, Kimball R, Goupee A. 2013 Wave basin model tests of floating offshore wind turbines. In *Proceedings of the ASME 2013 32nd International Conference on Ocean, Offshore and Arctic Engineering* (*OMAE 2013*), *Nantes, France, 9–14 June 2013*, p. V008T09A004. New York, NY: American Society of Mechanical Engineers.
44. Bredmose H, Larsen SE, Matha D, Rettenmeier A, Marino E, Saettran L. 2012 *Collation of offshore wind-wave dynamics*. Deliverable, MARINET: See http://www.fp7-marinet.eu/public/docs/D2.04_Collation_of_Offshore_Wind-Wave_Dynamics.pdf. Q4
45. Hansen AM, Laugesen R, Bredmose H, Mikkelsen R, Psichogios N. 2014 Small scale experimental study of the dynamic response of a tension leg platform wind turbine. *J. Renew. Sust. Energy* **6**, 053108. (doi:10.1063/1.4896602)
46. Masciola M, Robertson A, Jonkman J, Coulling A, Goupee A. 2013 Assessment of the importance of mooring dynamics on the global response of the DeepCwind floating semisubmersible offshore wind turbine. In *Proceedings of the Twenty-third* (*2013*) *International Offshore and Polar Engineering* (*ISOPE 2013*), *Anchorage, USA, 30 June–4 July 2013*, pp. 315–322. Mountain View, CA: International Society of Offshore and Polar Engineers.
47. Bottasso C, Campagnolo F, Petrovic V. 2014 Wind tunnel testing of scaled wind turbine models: Beyond aerodynamics. *J. Wind Eng. Ind. Aerodyn.* **127**, 11–28. (doi:10.1016/j.jweia.2014.01.009)
48. Campagnolo F, Bottasso CL, Bettini P. 2014 Design, manufacturing and characterization of aero-elastically scaled wind turbine blades for testing active and passive load alleviation techniques within a ABL wind tunnel. *J. Phys.* **524**, 012061. (doi:10.1088/1742-6596/524/1/012061)
49. Bayati I, Belloli M, Ferrari D, Fossati F, Giberti H. 2014 Wind tunnel tests on floating offshore wind turbines: design of A 6-DOD robotic platform for floating motion simulation. In *Proceedings of the EWEA, Barcelona, Spain, 10–13 March 2014*. Brussels, Belgium: European Wind Energy Association.
50. Utsunomiya T, Sato T, Matsukuma H, Yago K. 2009 Experimental validation for motion of a SPAR-type floating offshore wind turbine using 1/22.5 scale model. In *Proceedings of the ASME 2009 28th International Conference on Ocean, Offshore and Arctic Engineering* (*OMAE 2009*), *Honolulu, USA, 31 May–5 June 2009*, pp. 951–959. New York, NY: American Society of Mechanical Engineers.
51. Hall M, Moreno J, Thiagarajan K. 2014 Performance specifications for real-time hybrid testing of 1:50-scale floating wind turbine models. In *Proceedings of the ASME 2014 33rd International Conference on Ocean, Offshore and Arctic Engineering* (*OMAE 2014*), *San Francisco, USA, 8–13 June 2014*, p. V09BT09A047. New York, NY: American Society of Mechanical Engineers.
52. Azcona J, Bouchotrouch F, González M, Garciandía J, Munduate X, Kelberlau F, Nygaard TA. 2014 Aerodynamic thrust modelling in wave tank tests of offshore floating wind turbines using a ducted fan. *J. Phys.* **524**, 012089. (doi:10.1088/1742-6596/524/1/012089)
53. Matha D, Fechter U, Kühn M, Cheng PW. 2011 Non-linear multi-body mooring system model for floating offshore wind turbines. In *Proceedings of European Offshore Wind Conference and Exhibition* (*EOW 2011*), *Amsterdam, The Netherlands, 29 November–1 December 2011*, S. 504–513. Brussels, Belgium: European Wind Energy Association.
54. Journée J, Massie W. 2001 *Offshore hydromechanics* (*1st Ausg.*). Delft, The Netherlands: Delft University of Technology.